Aip1p Interacts with Cofilin to Disassemble Actin Filaments

Avital A. Rodal,* Jonathan W. Tetreault,† Pekka Lappalainen,§ David G. Drubin,* and David C. Amberg§

*Department of Molecular and Cell Biology, University of California at Berkeley, Berkeley, California 94720; †State University of New York Health Science Center, Department of Biochemistry and Molecular Biology, Syracuse, New York 13210; and §Institute of Biotechnology, 00014 University of Helsinki, Finland

Abstract. Actin interacting protein 1 (Aip1) is a conserved component of the actin cytoskeleton first identified in a two-hybrid screen against yeast actin. Here, we report that Aip1p also interacts with the ubiquitous actin depolymerizing factor cofilin. A two-hybrid–based approach using cofilin and actin mutants identified residues necessary for the interaction of actin, cofilin, and Aip1p in an apparent ternary complex. Deletion of the *AIP1* gene is lethal in combination with cofilin mutants or *act1-159*, an actin mutation that slows the rate of actin filament disassembly in vivo. Aip1p localizes to cortical actin patches in yeast cells, and this localization is disrupted by specific actin and cofilin mutations. Further, Aip1p is required to restrict cofilin localization to cortical patches. Finally, biochemical analyses show that Aip1p causes net depolymerization of actin filaments only in the presence of cofilin and that cofilin enhances binding of Aip1p to actin filaments. We conclude that Aip1p is a cofilin-associated protein that enhances the filament disassembly activity of cofilin and restricts cofilin localization to cortical actin patches.

Key words: Aip1 • cofilin •actin • cytoskeleton •*Saccharomyces cerevisiae*

THE actin cytoskeleton plays diverse roles in the cell, mediating such processes as endocytosis, exocytosis, cell motility, cell polarity, and cytokinesis in a spatially and temporally controlled manner. Each of these processes requires the regulation of specific dynamic properties and spatial organization of actin filaments by a subset of a large collection of actin-binding proteins. To determine how actin and associated proteins function together to control morphogenetic events, it will be important to determine how actin-associated proteins are sorted to different structures of the cytoskeleton, and how the combined actions of different actin-associated proteins affect cytoskeleton dynamics in these different structures.

Saccharomyces cerevisiae presents excellent opportunities for the study of combined effects of actin-associated proteins on actin assembly and organization both in vivo and in vitro. The actin cytoskeleton of *S. cerevisiae* is organized into polarized cortical patches and cytoplasmic bundles of actin filaments aligned along the mother–daughter cell axis (Adams and Pringle, 1984; Amberg, 1998). Little is known about how actin-binding proteins are sorted between different compartments of the cytoskeleton, or whether they themselves are responsible for forming these specialized actin networks.

We previously described a two-hybrid approach for characterizing interactions of actin-binding proteins with yeast actin (Amberg et al., 1995a). We used this system to identify yeast actin–associated proteins and examined their ability to interact with 35 clustered-charged-to-alanine mutants of actin. Those mutations that disrupt the binding of a particular ligand can identify regions of the actin surface important for a given interaction and can delineate an interaction footprint when displayed on the structure of actin. Actin interacting protein 1 (Aip1p),[1] identified in our two-hybrid analysis using actin as bait, had a very distinct interaction footprint on actin subdomains III and IV. We report here that in addition to interacting with actin, Aip1p also associates with the small actin-binding protein cofilin.

Members of the cofilin/actin depolymerizing factor family are conserved actin monomer and filament binding proteins that induce actin filament disassembly (for review see Moon and Drubin, 1995). Yeast cofilin is 40% identical in sequence to mammalian cofilin/actin depolymerizing factor; the gene is essential in yeast and the gene product localizes to cortical actin patches (Moon et al. 1993). Recently, two advances have led to a greater understanding of cofilin function in yeast: (1) A synoptic set of cofilin mu-

Address correspondence to David C. Amberg, State University of New York Health Science Center, Department of Biochemistry and Molecular Biology, Syracuse, NY 13210. Tel.: (315) 464-8727. Fax: (315) 464-8750. E-mail: ambergd@vax.hscsyr.edu

1. *Abbreviations used in this paper:* AD, activation domain; Aip1, actin interacting protein 1; 3-AT, 3,5-amino-triazole; DBD, DNA binding domain; GST, glutathione-*S*-transferase.

tants was constructed by alanine scanning mutagenesis (Lappalainen and Drubin, 1997) and (2) the structure of yeast cofilin was determined (Federov at al. 1997).

In this report, we have used this large set of genetic and structural tools in conjunction with classical biochemical and cell biological analyses to gain insight into the function of the interactions between Aip1p, cofilin, and actin. We found that Aip1p mediates the restriction of cofilin to cortical actin patches and that purified Aip1p has dramatic effects on cofilin's activity in vitro. Our results suggest that these two proteins interact in vivo to regulate actin dynamics.

Materials and Methods

Yeast Strains, Media, and Genetic Methods

Yeast strains are listed in Table I. FY23 and FY86 were provided by Fred Winston (Harvard Medical School, Boston, MA). Y187 and Y190 were provided by Steve Elledge (Baylor College of Medicine, Houston, TX). DDY319, DDY321, DDY760, and DDY496 were constructed as described (Holtzman et al., 1993, 1994; Moon et al., 1993). Standard methods were employed for growth, sporulation, and tetrad dissection of yeast (Rose et al., 1989). Yeast transformations were performed by electroporation (Becker and Guarente, 1991) or by lithium acetate (Rose et al., 1989). The medium for two-hybrid analysis was synthetic medium plus dextrose supplemented with adenine to 10 μg/ml and 3,5-amino-triazole (3-AT) (Sigma Chemical Co.) at 25, 50, or 100 mM.

Plasmid Construction and DNA Manipulations

Plasmid pRB2247 was constructed by isolating a 1.4-kb product of a BglII partial digest of plasmid pRB2248 and cloning this fragment into the BamHI site of plasmid pGEX-5X-3 (Pharmacia Biotech, Inc.) such that the *AIP1* gene was in frame with the glutathione-*S*-transferase (GST) reading frame. Plasmid pRB2251 was constructed by subcloning a 2.2-kb ClaI fragment from *AIP1* genomic clone pRB2249 into YCp50 such that *AIP1* and *bla* transcription is divergent. The deletion allele of *AIP1* was constructed by double fusion PCR and has been described elsewhere (Amberg et al., 1995b).

Plasmids encoding fusions of the *GAL4* DNA binding domain (DBD) to *SNF1* (pSE1112), the *GAL4* DBD to lamin (pAS1-lamin), and the *GAL4* activation domain (AD) to *SNF4* (pSE1111) were provided by Steve Elledge. The construction of the plasmids carrying fusions of the actin–alanine scan alleles to the Gal4 DBD, a fusion of the *GAL4* DBD to *ACT1* (pRB1516 also known as pDAb7), a fusion of the *GAL4* AD to *ACT1* (pAIP70), and a fusion of the *GAL4* AD to *AIP1* (pRB2248) previ-

Table I. Saccharomyces cerevisiae Strains

Name	Genotype	Source
FY23	*a ura3-52 leu2Δ1 trp1Δ63*	Winston et al., 1995
FY86	*α ura3-52 leu2Δ1 his3Δ200*	Winston et al., 1995
FY23×86	*a/α ura3-52/ura3-52 leu2Δ1/leu2Δ1 trp1Δ63/TRP1 HIS3/his3Δ200*	This work
Y187	*α gal4 gal80 his3 trp1-901 ade2-101 ura3-52 leu2-3,112 GAL--lacZ*	Bai and Elledge, 1996
Y190	*a gal4 gal80 his3 trp1-901 ade2-101 ura3-52 leu2-3,112 URA3::GAL--lacZ LYS2::GAL--HIS3cyh^r*	Bai and Elledge, 1996
DAY30	*a ura3-52 leu2Δ1 trp1Δ63 aip1-Δ1::URA3*	This work
DAY52	*a ura3-52 leu2Δ1 trp1Δ63 his3Δ200 aip1-Δ1::TRP1*	This work
DAY53	*a ura3-52 leu2Δ1 trp1Δ63 his3Δ200 aip1-Δ1::TRP1*	This work
DBY6527	*a ura3-52 leu2Δ1 trp1Δ63 his3Δ200 aip1-Δ1::URA3*	Amberg et al., 1995b
DBY6529	*a ura3-52 leu2Δ1 trp1Δ63 his3Δ200 aip1-Δ1::LEU2*	Amberg et al., 1995b
DBY6531	*α ura3-52 leu2Δ1 trp1Δ63 his3Δ200 aip1-Δ1::TRP1*	Amberg et al., 1995b
DDY130	*a ura3-52 leu2-3,112 his3Δ200 lys2-801*	
DDY496	*α leu2-3,112 ura3-52 sla2-Δ1::URA3*	
DDY319	*a sac6-Δ1::LEU2 his3Δ200 leu2-3,112 lys2-801 ura3-52*	
DDY321	*a abp1-Δ1::LEU2 his3Δ200 leu2-3,112 ura3-52*	
DDY760	*a sla1-Δ1::LEU2 leu2-3,112 ura3-52 ade2-1 ade3*	
TDS143	*a ura3-52 leu2-3,112 his3Δ200 tub2-210 act1-111::HIS3 ade4*	Wertman et al., 1992
TDS150	*a ura3-52 leu2-3,112 his3Δ200 tub2-210 act1-119::HIS3 ade4*	Wertman et al., 1992
TDS156	*a ura3-52 leu2-3,112 his3Δ200 tub2-210 act1-125::HIS3 ade4*	Wertman et al., 1992
TDS363	*a ura3-52 leu2-3,112 his3Δ200 tub2-210 act1-133::HIS3 ade2-101*	Wertman et al., 1992
TDS167	*a ura3-52 leu2-3,112 his3Δ200 tub2-210 ACT1::HIS3 ade4*	Wertman et al., 1992
DDY355	*a ura3-52 leu2-3,112 his3Δ200 tub2-210 act1-112::HIS3 ade4 ade2-101 cry1*	
DDY582	*a ura3-1 leu2-3,112 trp1-1 his3-11,15 ade2-101 cap2-Δ1::HIS3*	
DDY1252	*α ura3-52 his3Δ200 lys2-801 COF1::LEU2*	
DDY1253	*α ura3-52 his3Δ200 lys2-801 cof1-4*	
DDY1254	*α ura3-52 his3Δ200 lys2-801 cof1-5*	
DDY1255	*α ura3-52 his3Δ200 lys2-801 cof1-6*	
DDY1256	*α ura3-52 his3Δ200 lys2-801 cof1-7*	
DDY1257	*α ura3-52 his3Δ200 lys2-801 cof1-10*	
DDY1258	*α ura3-52 his3Δ200 lys2-801 cof1-8*	
DDY1259	*α ura3-52 his3Δ200 lys2-801 cof1-11*	
DDY1260	*α ura3-52 his3Δ200 lys2-801 cof1-12*	
DDY1261	*α ura3-52 his3Δ200 lys2-801 cof1-13*	
DDY1262	*α ura3-52 his3Δ200 lys2-801 cof1-15*	
DDY1263	*α ura3-52 his3Δ200 lys2-801 cof1-18*	
DDY1264	*α ura3-52 his3Δ200 lys2-801 cof1-19*	
DDY1265	*α ura3-52 his3Δ200 lys2-801 cof1-21*	
DDY1266	*α ura3-52 his3Δ200 lys2-801 cof1-22*	
DDY1435	*a ura3-52 leu2-3,112 his3Δ200 ade2-101 twf1Δ::URA3*	Goode et al., 1998
DDY1492	*a ura3-52 leu2-3,112 his3Δ200 tub2-101 act1-159::HIS3*	Belmont et al., 1998

ously were described elsewhere (Amberg et al., 1995a). The plasmid encoding a fusion of the *GAL4* DBD to *AIP1* (pDAb189) was constructed by removing the *AIP1* open reading frame from pRB2248 as a BglII partial digest and cloning it into the BamHI site of plasmid pRB1516 (Amberg et al., 1995a) (a Cen version of pAS1-CYH2) so that the *AIP1* open reading frame is in frame with that of the *GAL4* DBD. The construct encoding a fusion of the *GAL4* AD to *ABP1* (pDAb20) was constructed by excising the *ABP1* open reading frame from plasmid pRB1199 (Drubin et al., 1988) as a 1.9-kb XhoI-EcoRI fragment, blunting the EcoRI site with T4 DNA polymerase and cloning into plasmid pACTII (gift of Steve Elledge) that had been cut with XhoI and SalI in which the SalI site had been made blunt with T4 DNA polymerase. The resulting construct expresses all but the first 11 amino acids of Abp1p fused to Gal4p.

The constructs encoding fusions of the cofilin mutants to the Gal4p AD (used for the footprinting studies) were constructed by PCR into plasmid pACTII. The cofilin mutant and wild-type alleles were amplified off plasmids (Lappalainen et al., 1997) using primers DAo-COF1-1 (5′-cgcgccatggaacaaaagatgtctagatct-3′) and DAo-COF1-2 (5′-cggaattcaccttaatgagaaccagcgcc-3′) and vent polymerase (New England Biolabs Inc.). Subcloning of *cof1-4* required the use of the special primer DAo-COF1-3 (5′-cgcgccatggaacaaaagatgtctagagct-3′) in the place of primer DAo-COF1-1. The PCR products were cut with NcoI and EcoRI and cloned into similarly cut pACTII. Each construct was cloned and tested in duplicates generated from separate PCR reactions. When possible, constructs were confirmed by a BbvI digest. Plasmid pACTII-COF1 was made by PCR amplification of the *COF1* open reading frame with oligonucleotides PL70 (5′-gcgcgccatggggtctagatctggtgttgctgttgc-3′) and PL76.2 (5′-gcgcgcggatccttaatgagaaccagcgcctctgc-3′), digestion of the PCR product with NcoI-BamHI, and subcloning of this insert in frame into similarly digested pACTII.

To express Aip1p as a GST fusion protein in yeast, primers ARP1 (5′-gcgcgggatccatgtcatctatctctttgaaggaa-3′) and ARP3 (5′-cgcgccggccgctcactcgaggacaacattccacct-3′) were used to amplify the *AIP1* open reading frame from genomic DNA. This PCR product was cleaved with BamHI and EagI and cloned into similarly cut pEG(KT) (Mitchell et al., 1993) to make plasmid pAR3.

To express Aip1p for in vitro translation, primers ARP16 (5′-gcgcgcacatgtatgtcatctatctctttgaaggaa-3′) and ARP4 (5′-gcgcgaagctttcactcgaggacaacattccacct-3′) were used to amplify the *AIP1* open reading frame from genomic DNA. This PCR product was cleaved with AflIII and HindIII and cloned into pBAT4 (Përanen et al., 1996) cut with NcoI and HindIII to make plasmid pAR20.

Protein Purification and Antibody Production

Aip1-GST fusion protein for antibody production was purified from bacterial strain UT5600 (Δ*[ompT-fepA] leu proC trpE*) (provided by S. Gottesman, National Cancer Institute, Bethesda, MD) carrying plasmid pRB2247 by standard methods (Smith and Johnson, 1988; GST Gene Fusion System manual, Pharmacia Biotech, Inc.). Antibodies were raised in three New Zealand white rabbits by injection of 100 μg GST-Aip1 in 1 ml of adjuvant (RIBI ImmunoChem Research Inc.), three times at 2-wk intervals. 2 wk after the last boost, the animals were exsanguinated. Anti-Aip1 antibodies were affinity-purified on columns to which GST-Aip1p had been conjugated by standard methods (Harlow and Lane, 1988). Purified antibodies were concentrated on a Centriplus concentrator (Amicon Inc.).

Yeast actin was purified as described previously (Goode et al., 1999). However, the formamide eluate from the DNaseI column was dialyzed overnight against three changes of G buffer (5 mM Tris, pH 7.5, 0.2 mM ATP, 0.2 mM DTT, 0.2 mM $CaCl_2$), and concentrated to 2 ml in Centriprep 10 devices (Amicon, Inc.). The actin was polymerized by adding initiation salts to a final concentration of 100 mM KCl, 2 mM $MgCl_2$, and incubating for 2 h at room temperature. Residual actin-binding proteins were stripped from F-actin at this point by slowly adding KCl to 0.6 M and further incubating for 30 min. The polymerized actin was pelleted at 80,000 rpm for 30 min at room temperature in a TLA100.3 rotor (Beckman Instruments, Inc.). The pelleted actin was resuspended in G buffer to a final concentration of 50 μM and dialyzed against three changes of 2 liters of G buffer before it was frozen in liquid N_2 and stored at −80°C. Cofilin was purified as a GST-fusion protein from *Escherichia coli* and subsequently cleaved from GST by thrombin digestion as described previously (Lappalainen et al., 1997).

Aip1p was purified from the yeast strain DDY130 (carrying the plasmid pAR3) as a GST fusion protein under the control of the GAL promoter. 4 liters of cells were grown at 30°C in synthetic medium with 2% dextrose and without uracil or leucine to an OD of 1.0 at 600 nm, harvested by centrifugation, and resuspended in 4 liters of synthetic medium with 2% glycerol and without uracil or leucine. After an overnight incubation at 30°C to derepress the galactose promoter, cells were again harvested and resuspended in 4 liters of rich medium with 2% galactose. The cultures were induced for 8 h at 30°C before cells were once again harvested, washed twice with 100 ml water, resuspended in 10 ml water, frozen as 50-μl pellets in liquid N_2, and stored at −80°C. Yeast pellets were lysed in liquid N_2 in a Waring blender and thawed in PBS to a final concentration of 1×, with 1 mM PMSF and 0.5 μg/ml each of antipain, leupeptin, pepstatin A, chymostatin, and aprotin. The lystate was cleared first by spinning at 17,000 *g* in a Dupont GSA rotor. The supernatant from this spin was cleared by spinning at 50,000 rpm for 50 min in a Beckman 70Ti rotor. This high speed supernatant was dialyzed overnight against PBS and passed twice over a column with a 4-ml bed of glutathione agarose beads (Sigma Chemical Co.). The column was washed five times with PBS and incubated with thrombin (5 U/ml; Sigma Chemical Co.) overnight at room temperature to cleave the Aip1p from the GST. The column was washed with 8 ml 50 mM Hepes, pH 7.2, 50 mM KCl, and the flow-through was concentrated to 2 ml and loaded onto a 1-ml mono-Q anion exchange column (Pharmacia Biotech Inc.). A linear salt gradient from 100 to 400 mM KCl was applied to the column and peak fractions containing Aip1p were concentrated to 15 μM, frozen in liquid N_2, and stored at −80°C.

Two-Hybrid Analyses

In all cases, two-hybrid analyses were performed by mating strain Y190 carrying constructs encoding fusions to the Gal4 DBD, to strain Y187 carrying constructs encoding fusions to the Gal4 AD. Transformants were lined, spotted, or spread as lawns on selective medium, synthetic complete medium lacking Trp (SC-TRP) or DBD fusions and synthetic complete medium lacking Leu (SC-LEU) for AD fusions. Mating was carried out by replica plating the Y190 and Y187 derivatives together onto yeast extract/peptone/dextrose medium–plates, incubating at 30°C for 24 h, selecting the mated cells on SC-TRP,-LEU. The selected diploids, carrying both DBD and AD fusion constructs, were replica plated to media containing 25, 50, and 100 mM 3-AT (Sigma Chemical Co.) and incubated at 25°C.

Microscopy

Immunofluorescence was performed by standard protocols using a methanol/acetone fixation (Pringle et al., 1991). Affinity-purified anti-Aip1p antibody was used at a dilution of 1:100. Affinity-purified rabbit anticofilin was used at 1:100. Guinea pig antiactin antisera (animal 2) (Mulholland et al., 1994) was used at 1:2,000. For Aip1p localization, FITC-conjugated goat anti–rabbit IgG (Organon Teknika Corp.) was used at 1:1,000 and rhodamine-conjugated goat anti–guinea pig (Organon Teknika Corp.) was used at 1:1,000. For Aip1p localization in wild-type and *act1-111* strains, rhodamine-conjugated goat anti–rabbit IgG (Cappel; ICN Biomedicals) was used at 1:1,000. For cofilin localization in DAY30 and DDY1264 FITC-conjugated goat anti–rabbit IgG (Cappel; ICN Biochemicals) was used at 1:1,000 and rhodamine-conjugated goat anti–guinea pig IgG (Cappel; ICN Biochemicals) was used at 1:1,000.

Actin Filament Sedimentation Assay

To evaluate actin filament sedimentation in the presence of Aip1p and cofilin, 3.75 μM actin was polymerized at room temperature in F-buffer (5 mM Tris, pH 7.5, 0.7 mM ATP, 0.2 mM $CaCl_2$, 2 mM $MgCl_2$, 100 mM KCl, 0.2 mM DTT). After 45 min, polymerized actin (final concentration, 2.5 μM) was added to variable concentrations of Aip1p (final concentration, 0.012–0.5 μM) and/or cofilin (final concentration, 0.125–0.5 μM) in F-buffer. The reactions were incubated at room temperature for 20 min and centrifuged at 90,000 rpm for 20 min at 23°C in a TLA100 rotor (Beckman Instruments) to pellet the actin filaments. Equal proportions of the pellets and supernatants were fractionated on 12% SDS-PAGE gels and proteins were visualized by Coomassie blue staining. Protein levels were quantified using NIH Image software.

F-Actin Binding Assay

To test the cofilin dependence of Aip1p binding to F-actin, variable concentrations of yeast F-actin were incubated for 20 min at 25°C with equimolar amounts of cofilin or control buffer. [^{35}S]Methionine-labeled in vitro–translated (TNT quick coupled transcription/translation; Promega

Corp.) Aip1p from plasmid pAR20 was incubated for 20 min with the cofilin–F-actin and pelleted for 20 min at 90,000 rpm in a TLA100 rotor (Beckman Instruments). Equal amounts of supernatants and pellets were fractionated on 13% SDS-PAGE gels and visualized by autoradiography. Results were quantified on a PhosphorImager using ImageQuant software (STORM 860; Molecular Dynamics, Inc.) and on an IS2000 densitometer using AlphaImager software.

Molecular Modeling

Images of actin and cofilin molecular models were generated on a Silicon Graphics Indigo™ workstation running Sybil software (Tripos Inc.). Coordinates for actin (file 1ATN) and yeast cofilin (file 1CFY) were retrieved from the Brookhaven database.

Results

Identification and Sequence of Aip1p

Aip1p was first identified as a 67-kD yeast protein that interacts with actin in the two-hybrid system (Amberg et al., 1995a; GenBank accession number P46680) and is the first discovered member of a family of conserved proteins (Fig.

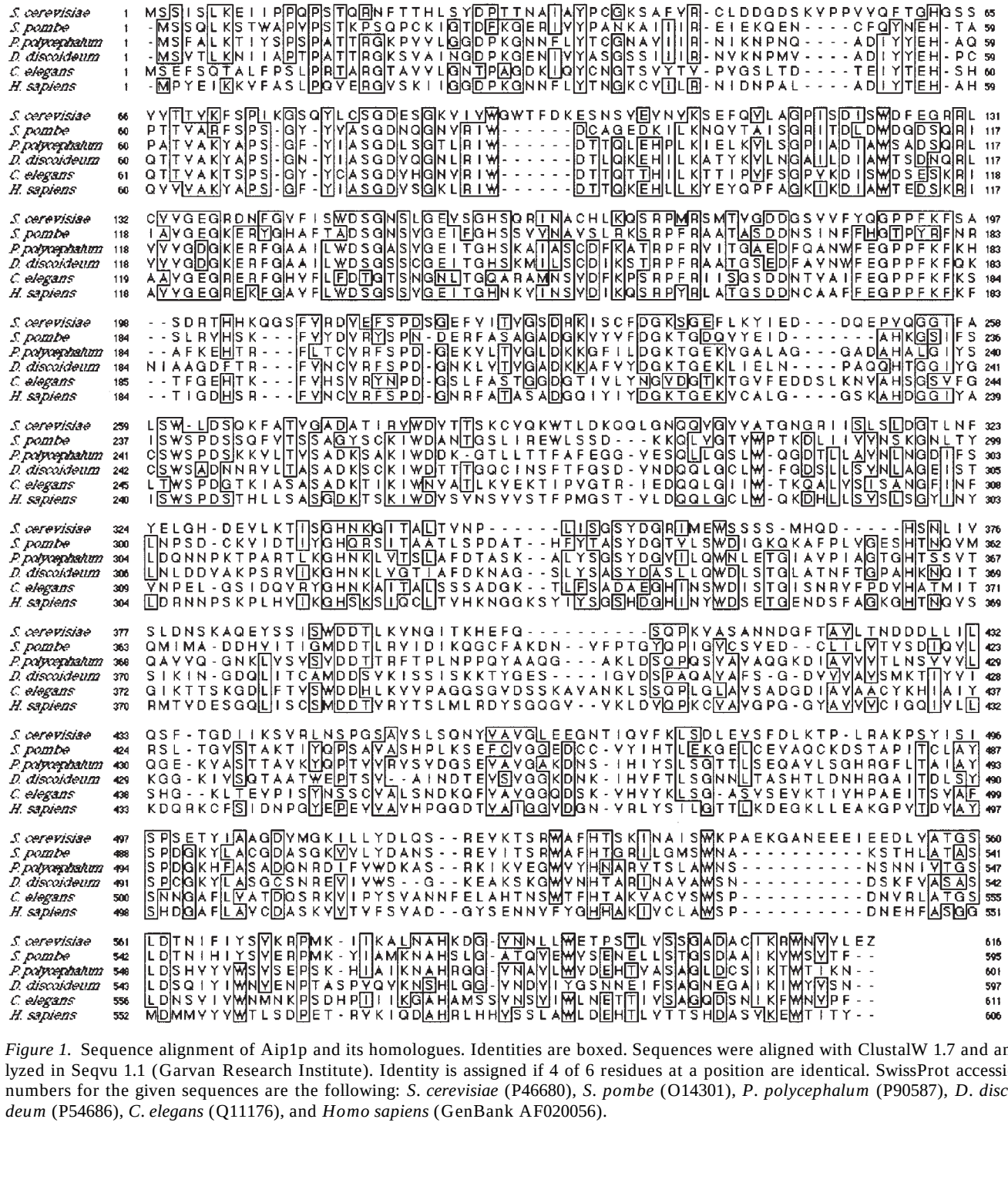

Figure 1. Sequence alignment of Aip1p and its homologues. Identities are boxed. Sequences were aligned with ClustalW 1.7 and analyzed in Seqvu 1.1 (Garvan Research Institute). Identity is assigned if 4 of 6 residues at a position are identical. SwissProt accession numbers for the given sequences are the following: *S. cerevisiae* (P46680), *S. pombe* (O14301), *P. polycephalum* (P90587), *D. discoideum* (P54686), *C. elegans* (Q11176), and *Homo sapiens* (GenBank AF020056).

1). Homologues of Aip1p have been identified in *Schizosaccharomyces pombe*, *Physarum polycephalum* (Matsumoto et al., 1998), *Dictyostelium discoideum*, *Caenorhabditis elegans* (where there are two homologues), *Mus musculus*, and humans. Additionally, members of the Aip1p family show weak homology to proteins that contain reiterated motifs called WD repeats. These repeats were first identified in β subunits of trimeric G-proteins (Fong et al., 1986) and have since been found in proteins with highly diverse functions. Members of the Aip1p family contain from four to eight WD repeats.

Two-Hybrid Interactions between Aip1p and Cofilin

To identify additional Aip1p ligands we used a two-hybrid construct of Aip1p fused to the *GAL4* DBD (plasmid pDAb189) to screen a large set of yeast actin interacting proteins and cell polarity proteins fused to the *GAL4* activation domain. Included in this set were clones encoding *AIP1*, *AIP2*, *AIP3*, *OYE2*, *SRV2*, *PFY1*, *COF1*, *BNR1*, *LAS17*, *MNN10*, *ABP1*, *RVS167*, *BEM1*, *FUS1*, and *SAC6*. As can be seen in Fig. 2, we found that in addition to actin, Aip1p also interacted with Cof1p (yeast cofilin). These interactions are specific since no activation was observed between Aip1p and the transcription factor Snf4p or between Aip1p and the actin cortical patch protein Abp1p (data not shown). Furthermore, the Aip1p–actin and Aip1p–cofilin two-hybrid interactions are reciprocal. An apparent cofilin–cofilin interaction also was detected but is likely the result of bridging through actin. The focus of this study is the functional significance of the Aip1p–cofilin interaction.

The Aip1p and Cofilin Binding Footprints on Actin

To obtain a structural framework for understanding the functions of the Aip1p–actin and cofilin–actin interactions, we used actin mutations (Wertman et al., 1992) in conjunction with the two-hybrid system to identify likely sites of interaction for these proteins on actin. This approach was described previously for the identification of the binding footprint of Aip1p on actin (Amberg et al., 1995a) and was repeated here to identify the binding footprint for cofilin on actin (Fig. 3, A and B and Table II).

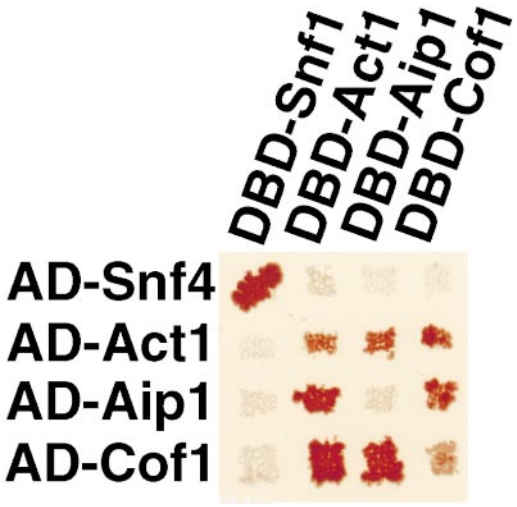

Figure 2. Two-hybrid interactions of Aip1p. A *GAL4*-based two-hybrid system was used to assess interactions between Aip1p and several proteins involved in cytoskeleton function and cell polarity. Displayed here is a representative sampling of that data. The two-hybrid plasmids were cointroduced by mating strain Y190, carrying plasmids encoding fusions to the *GAL4* DBD, and strain Y187, carrying plasmids encoding fusions to the *GAL4* AD. The resulting diploids were selected and replica plated to medium containing 100 mM 3-AT.

Yeast strain Y187, carrying a fusion of the Gal4p AD to cofilin, was mated to strain Y190 containing plasmids encoding fusions of 35 actin mutants to the Gal4p DBD (Amberg et al., 1995a). Diploids were replica plated on 3-AT medium to assess activation of the His3p two-hybrid reporter (Fig. 3 A). Failure to grow on this medium indicates that the actin mutant contained in that strain is defective for the cofilin–actin interaction. This result suggests that the mutation may lie in or near the cofilin binding site on actin. We discovered that eight actin mutants failed to interact with cofilin (Fig. 3 A). Of these eight, five have thus far failed to interact with any actin-binding protein tested (*act1-107*, *act1-130*, *act1-127*, *act1-128*, and *act1-108*) and probably encode either unfolded or unstable proteins. Therefore, nothing can be concluded from these mutants. However, the remaining three mutants (*act1-103*, *act1-106*, and *act1-126*) display specific effects on the cofilin–actin interaction (Fig. 3 A).

The three mutations that specifically disrupt the cofilin–actin interaction are located in a small region of subdomain III on actin. Interestingly, these three mutations form one-half of the Aip1p binding footprint (Amberg et al., 1995a) that includes *act1-109*, *act1-111*, and *act1-112*, as well as *act1-103*, *act1-106*, and *act1-126* (Fig. 3 B). These data are consistent with the model that Aip1p binding to actin is facilitated by cofilin.

The Aip1p and Actin Binding Footprints on Cofilin

A large set of mutant alleles of cofilin has been constructed (Lappalainen et al., 1997) and the yeast cofilin structure has been determined (Federov et al., 1997). This presented us with the opportunity to use our two-hybrid methodology to identify surfaces on cofilin required for its interactions with Aip1p and actin. Toward this end, we cloned the cofilin mutants into the two-hybrid activation domain vector pACTII (gift of S. Elledge) and scored the ability of these mutants to interact with Aip1p and actin. Four cofilin mutants failed to interact with both actin and Aip1p: *cof1-9*, *cof1-16*, *cof1-17*, and *cof1-20*. Two cofilin mutants specifically failed to interact with actin: *cof1-6* and *cof1-14*. Three mutants, *cof1-4*, *cof1-13*, and *cof1-22*, failed to interact with Aip1p but interacted well with actin.

We displayed the two-hybrid data on the molecular model of cofilin (Fig. 3, C and D). In agreement with the in vitro binding data of cofilin mutants to actin (Lappalainen et al., 1997), the two-hybrid data identified a ridge that is involved in the actin interaction (Fig. 3, red and purple in B and C), on the edge of the disc-shaped cofilin protein. A subset of the mutations that disrupted the cofilin–actin interaction constitute part of the Aip1p footprint on cofilin (shown in purple in Fig. 3, C and D). A different set of mutations specifically affected cofilin interactions with Aip1p and not actin (shown in blue). These data are consistent

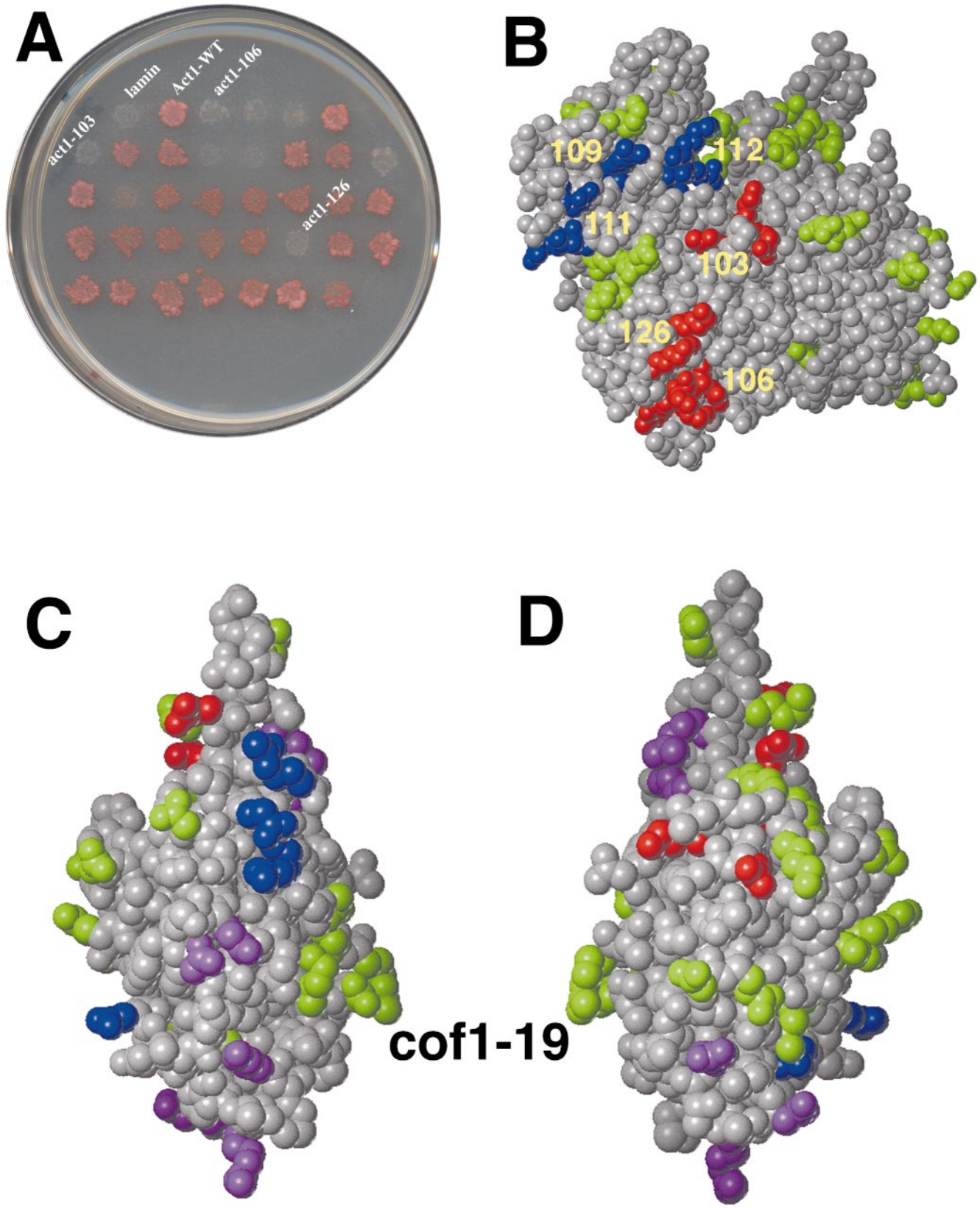

Figure 3. Two-hybrid analysis of the structure of the Aip1p–cofilin–actin complex. Two-hybrid analysis was performed between 36 actin alleles fused to the *GAL4* DBD and cofilin fused to the *GAL4* AD. Activation of the *HIS3* two-hybrid reporter was assessed on medium containing 50 mM 3-AT at 25°C (A). A model of the actin monomer is shown in B. In red are the amino acids altered by mutations that disrupt both the actin–cofilin and actin–Aip1p two-hybrid interactions. In blue are the amino acids altered by mutations that disrupt only the actin–Aip1p interaction. Marked with green are those mutations that had no effect on either interaction. The allele numbers of disruptive mutations are indicated. Displayed in C and D are two views, 180° apart, of yeast cofilin. Mutations that disrupted both the cofilin–actin and the cofilin–Aip1p two-hybrid interactions are indicated in purple. Mutations that disrupted the cofilin–actin interaction alone are indicated in red. Mutations that disrupted the cofilin–Aip1p interaction alone are indicated in blue, and mutations that had no effect on either the cofilin–actin or cofilin–Aip1 interactions are shown in green.

Table II. Genetic and Physical Interactions within the Aip1p-Cof1p-Act1p Complex

Allele	Phen.	Two-hybrid interactions		Genetic interactions	Localization	
		With actin	With Aip1p		Aip1p localization	Cof1p localization
COF1	*WT*	+++	+++	na	Cortical patches	Cortical patches
cof1-4	wt	+++	−	SL w/aip1Δ	Cortical patches	Cortical patches
cof1-5	ts	+++	+++	SL w/aip1Δ	Cortical patches	Cortical patches
cof1-6	wt	−	++	ts w/aip1Δ	Cortical patches	Cortical patches
cof1-7	nd	+++	+++	nd	nd	nd
cof1-8	ts	++	+	nd	Cortical patches	Cortical patches
cof1-9	lt	−	−	nd	nd	nd
cof1-10	wt	+++	+++	None	Cortical patches	Cortical patches
cof1-11	wt	+++	+++	None	Cortical patches	Cortical patches
cof1-12	wt	+++	+++	None	Cortical patches	Cortical patches
cof1-13	wt	+++	−	None	Cortical patches	Cortical patches
cof1-14	lt	−	++	nd	nd	nd
cof1-15	wt	++	+++	None	Cortical patches	Cortical patches
cof1-16	lt	−	−	nd	nd	nd
cof1-17	lt	−	−	nd	nd	nd
cof1-18	wt	+++	+++	nd	Cortical patches	Cortical patches
cof1-19	wt	++	++	None	Cytosolic	Patches and cables
cof1-20	lt	−	−	None	nd	nd
cof1-21	wt	+++	+++	nd	Cortical patches	Cortical patches
cof1-22	ts	++	−	SL w/aip1Δ	Cortical patches	Cortical patches
aip1Δ	wt	na	na	SL w/act1-159	na	Patches and cables
act1-111	ts	na	−	na	Cytosolic	Patches
act1-112	ts	na	−	na	Mostly cytosolic	Patches

Abbreviations: wt, wild-type; ts, temperature sensitive; lt, lethal; na, not applicable; SL, synthetic lethal; nd, no data. Genetic interactions were determined from dissection of eight tetrads derived from two different complex heterozygotes. The tetrads were incubated at 25°C and the genotypes of the spore strains were inferred from marker segregation. None of the double mutants were viable for combinations scored as showing synthetic lethality. Double mutants that were viable at 25°C were grown at a variety of temperatures and compared in parallel with sibling spores from the same tetrads (including single mutants) to determine temperature sensitivity. 27 of 29 *aip1Δcof1-6* isolates were temperature sensitive at 37°C.

with the model that Aip1p binding to cofilin is facilitated by actin because, according to this model, disruption of the cofilin–actin interaction would be predicted to also disrupt the Aip1p–cofilin interaction. Overall, the footprinting data suggest that there is a ternary complex between Aip1p, cofilin, and actin, and that the members of this complex make distinct contacts with each other.

Synthetic Interactions with aip1Δ Mutants

The actin cytoskeleton consists of a large number of interacting components. Often the deletion of a gene encoding one of these components does not in itself cause a readily detectable phenotype. However, combinations of mutations can produce informative synthetic phenotypes that suggest a shared or parallel function for the proteins involved (Adams et al., 1993). Deletion of the *AIP1* gene had no effect on cell growth on a variety of media at a variety of temperatures (data not shown). Therefore, we investigated its genetic interactions with mutations in genes that encode other actin-binding proteins.

First we crossed the *aip1Δ* strain to the collection of clustered-charged-to-alanine mutants of *COF1* (*cof1-4*, *cof1-5*, *cof1-6*, *cof1-7*, *cof1-10*, *cof1-11*, *cof1-12*, *cof1-13*, *cof1-15*, *cof1-18*, *cof1-19*, *cof1-21*, and *cof1-22*). The results of these crosses are shown in Table II. The *aip1Δ* mutation is synthetically lethal with *cof1-5* and *cof1-22*, which are both temperature sensitive for growth on their own and show defects in actin turnover rates in vivo at the permissive temperature (Lappalainen and Drubin, 1997). In addition, the *aip1Δ* mutant is synthetically lethal with *cof1-4*, which has no growth phenotype of its own but has actin organization defects as visualized by rhodamine-phalloidin staining (Lappalainen et al., 1997). The *aip1Δ* mutant is also synthetically temperature sensitive at 37°C with *cof1-6*, which has no actin organization or growth phenotype on its own (Lappalainen et al., 1997). We examined actin and cofilin localization in the *aip1Δ cof1-6* double mutant. At the permissive temperature, the double mutant grows slowly and has actin clumps in the mother cell. These clumps stain with rhodamine-phalloidin, which binds specifically to F-actin and not G-actin. At the restrictive temperature, actin is depolarized, actin clumps are apparent, and unbudded cells accumulate. Cofilin colocalizes with the actin structures at both the permissive and restrictive temperatures (data not shown).

We also determined if the *aip1Δ* mutation displayed synthetic lethality with any of the viable actin–alanine scan alleles of actin (*act1-1*, *-101*, *102*, *104*, *105*, *108*, *111*, *113*, *115*, *116*, *117*, *119*, *120*, *121*, *122*, *123*, *124*, *125*, *129*, *132*, *133*, *136*) and *act1-159*, which decreases rates of actin filament turnover in vivo and in vitro (Belmont et al., 1998). When a yeast strain carrying the *act1-159* mutation was crossed to the *aip1Δ* strain, double mutant spores failed to grow at 25°C. We also observed subtle synthetic growth defects in double mutants containing the *aip1Δ* allele and three other actin alleles: *act1-133*, *act1-119*, and *act1-125* (data not shown). These three mutations are not located near the Aip1p interaction interface on actin (Fig. 3), suggesting that the weak synthetic interactions are not a function of compromised Aip1p–actin interactions but of cumulative defects in cytoskeletal function.

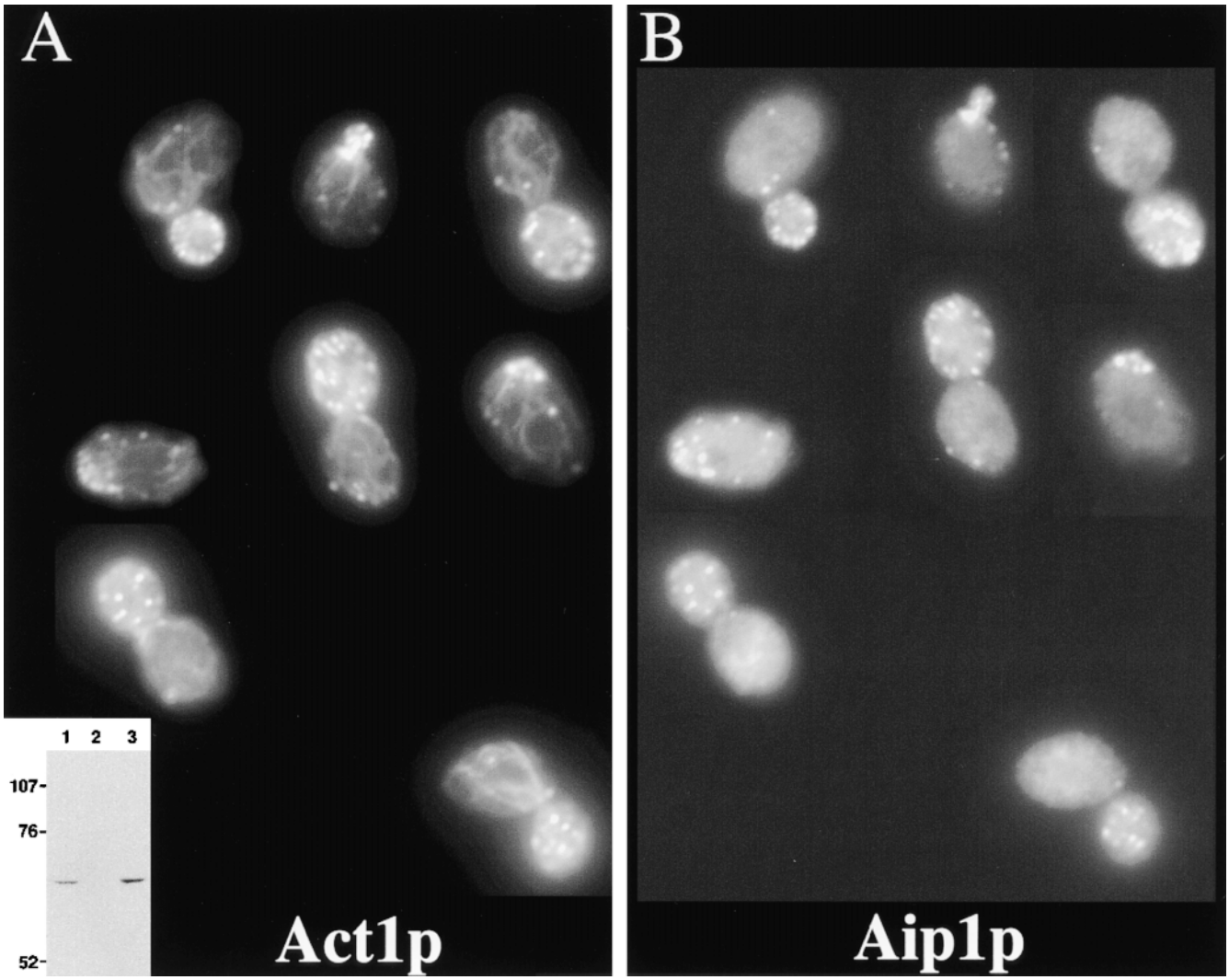

Figure 4. Aip1p localizes to cortical actin patches. Immunofluorescence was performed on wild-type strain FY23×86 using a guinea pig antiactin antibody (A) and affinity-purified anti-Aip1 antibody (B). Western blot of yeast protein extracts using anti-Aip1p rabbit antiserum (insert in A). The amount of protein loaded was normalized to the number of cells from which extract was prepared. Wild-type strain FY23 (lane 1), *AIP1* deletion strain DAY53 (lane 2). DAY53 carrying plasmid pRB2251 with a minimal genomic subclone of the *AIP1* locus (lane 3).

Finally, we determined if the *aip1Δ* allele was synthetically lethal with deletion alleles of six other components of the yeast cortical cytoskeleton: *ABP1*, *SLA1*, *SLA2*, *TWF1*, *CAP2*, and *SAC6*. No clear synthetic lethality was found. However, the *sac6*Δ, *cap2*Δ*-1*, and *sla1*Δ mutations had slight synthetic growth defects in combination with the *aip1Δ* allele (data not shown).

Aip1p Localizes to Cortical Actin Patches

As a further test of the importance of the Aip1p–actin and Aip1p–cofilin interactions in vivo, we sought to determine if Aip1p colocalizes with actin and cofilin. Toward this end, we generated antibodies to a GST-Aip1p fusion protein. These antibodies specifically recognize a 67-kD protein on Western blots of wild-type (FY23) yeast extract (Fig. 4 A, inset, lane 1) that is of the expected size based on the primary sequence of *AIP1*. This band is absent from *AIP1* deletion strain DAY53 (Fig. 4 A, inset, lane 2), but is restored when a low copy number vector carrying a 2.2-kb *AIP1* genomic fragment (pRB2251) is introduced into the deletion strain (Fig. 4 A, inset, lane 3).

Wild-type strain FY23×86 was stained with the anti-Aip1p antibodies (Fig. 4 B) and guinea pig antiactin antibodies (Fig. 4 A). Aip1p localized only to cortical actin patches and was not detected along the actin cables. This localization pattern is identical to that observed for cofilin (Moon, 1993), but simultaneous colocalization of Aip1p and cofilin was not possible, since both antibodies were raised in rabbits. Since both Aip1p and cofilin appear to be found in all actin cortical patches recognizable by antiactin antibodies, we presume that Aip1p and cofilin colocalize. Aip1p also localized diffusely throughout the cytoplasm and this cytoplasmic staining is not seen in the *aip1Δ* strain (data not shown).

The Aip1p–Actin Interaction Is Required for Aip1p Localization to Cortical Patches

To assess the importance and relevance of the Aip1p–actin two-hybrid interaction, we localized Aip1p in a strain bearing actin mutations that disrupt the Aip1p–actin two-hybrid interaction. Fig. 5 A shows Aip1p localization in the *act1-111* strain TDS143. Aip1p was not detected in cortical patches in the mutant strain and there is an apparent increase in the cytosolic Aip1p signal. The failure of Aip1p to localize in this strain is not due to a loss in the ability of cofilin to bind to actin (Fig. 5 B). Similarly, Aip1p localization to cortical patches in an *act1-112* strain is severely compromised (Fig. 5 C), whereas cofilin localization to patches in this strain is not affected (Fig. 5 D). Aip1p was well localized to cortical patches in *act1-119*, *act1-132*, *act1-124*, and *act1-125* strains (data not shown) indicating that Aip1p mislocalization is not caused by generalized defects in the actin cytoskeleton. These results suggest that Aip1p must bind to F-actin for stable association with cortical actin patches and is consistent with the two-hybrid data suggesting that Aip1p contacts actin in the vicinity of the *act1-111* and *act1-112* mutations.

Aip1p Localization in Cofilin Mutants

To test the importance of the Aip1p–cofilin interaction on Aip1p localization, we examined Aip1p localization in viable cofilin mutants (Lappalainen et al., 1997). Both Aip1p and cofilin were localized by indirect immunofluorescence in strains bearing 14 different *cof1* alleles: *cof1-4*, *cof1-5*, *cof1-6*, *cof1-7*, *cof1-8*, *cof1-10*, *cof1-11*, *cof1-12*, *cof1-13*, *cof1-15*, *cof1-18*, *cof1-19*, *cof1-21*, *cof1-22*, and a wild-type congenic strain (Table II). The cells were grown at 25°C, a permissive temperature for all the strains, before fixation. Aip1p localized to patches in all of the cofilin mutants except the strain carrying the *cof1-19* allele. Fig. 5 E shows Aip1p localization in *cof1-19* strain DDY1264. As was seen with the *act1-111* strain, Aip1p is lost completely from the cortical patches in *cof1-19* cells and there is an apparent increase in the cytoplasmic pool of Aip1p. Double labeling of this strain with antiactin and anticofilin antibodies showed that Cof1-19p is associated with cortical actin patches (Fig. 6).

The *cof1-19* strain, like the *aip1Δ* strain, is viable and has a wild-type growth phenotype. We have examined the actin cytoskeleton in these strains and found no obvious defects. However, both strains do appear to have slightly aberrant cortical actin patches: they appear by rhodamine-phalloidin staining to be slightly larger or perhaps to contain more F-actin (data not shown). In addition, the *cof1-19* cells have slightly depolarized actin patches and misoriented actin cables.

Aip1p is Required for Normal Cofilin Localization

To examine the role of Aip1p in cofilin localization, we immunolocalized cofilin in the *aip1Δ* strain. Surprisingly, cofilin localized not only to cortical patches but also to actin cables (Fig. 6 D). We confirmed colocalization of cofilin with actin cables by double staining with the guinea pig antiactin antibody, as shown in Fig. 6 C. This result suggests that Aip1p is required to restrict cofilin to cortical actin patches in the yeast actin cytoskeleton.

We asked if exclusive localization of cofilin to cortical actin patches depends on localization of Aip1p to these patches. To address this question, we examined cofilin localization in the *cof1-19* mutant strain DDY1264, in which Aip1p is localized in the cytoplasm. As can be seen in Fig. 6 F, Cof1-19p is localized to both the patches and the cables. Fig. 6 E shows the same cells stained with the antiactin antibody confirming association of Cof1-19p with the actin cables. Though *act1-111* and *act1-112* mutants also fail to localize Aip1p to actin patches (Fig. 5), we were unable to confirm that cofilin also localizes to actin cables in these strains because their actin cytoskeletons are more generally disrupted and cables are undetectable by antibody staining (data not shown).

We next asked if the localization of other proteins normally localized to the cortical actin patches was affected in the *aip1Δ* strain. We found that immunolocalization of Abp1p, fimbrin/Sac6p, and coronin/Crn1p was unaffected by the absence of Aip1p (data not shown). This indicates that the role of Aip1p in cofilin localization is specific and not reflective of gross structural defects in the cortical patches.

Aip1p Increases the Extent of Cofilin-induced Depolymerization

To evaluate directly the functional and physical interaction between cofilin, actin, and Aip1p, we investigated the effects that these proteins might have together in vitro. Aip1p was expressed in yeast as a GST fusion protein under the control of the *GAL* promoter. GST–Aip1p was affinity-purified from extracts on glutathione-agarose beads, cleaved from GST by thrombin digestion, and purified by cation exchange chromatography. This protein has two additional amino acids NH_2-terminal to the primary sequence of Aip1p. No contaminants are apparent in the preparation on overloaded (5 μg) Coomassie stained gels (data not shown).

To evaluate the interaction of Aip1p with F-actin at steady state, we carried out cosedimentation assays with 2.5 μM prepolymerized yeast F-actin. For all of the assays described here, after 20 min of coincubation the reaction is at steady state as evaluated by light-scattering at 400 nm (data not shown). Although a small proportion (5–10%) of purified Aip1p sedimented in the absence of actin in these assays, this amount did not perceptibly increase upon addition of actin (data not shown). Given the two-hybrid interaction of Aip1p and cofilin, it seemed possible that an actin–Aip1p interaction might be mediated by cofilin. To test this hypothesis, we performed the cosedimentation assay in the presence of recombinant cofilin, which binds to F-actin and accelerates disassembly rates (increasing subunit turnover), but does not significantly change actin polymer levels at steady state (Fig. 7 B, lanes 1 and 2). Strikingly, in the presence of both Aip1p and cofilin, we observed a dramatic shift of actin and cofilin from the pellet to the supernatant (Fig. 7 A, lane 2). This shift might be explained by invoking a monomer sequestering model as applies for twinfilin (Goode et al., 1998), a protein that binds stoichiometrically to actin monomer, preventing nucleotide exchange and polymerization. We examined the

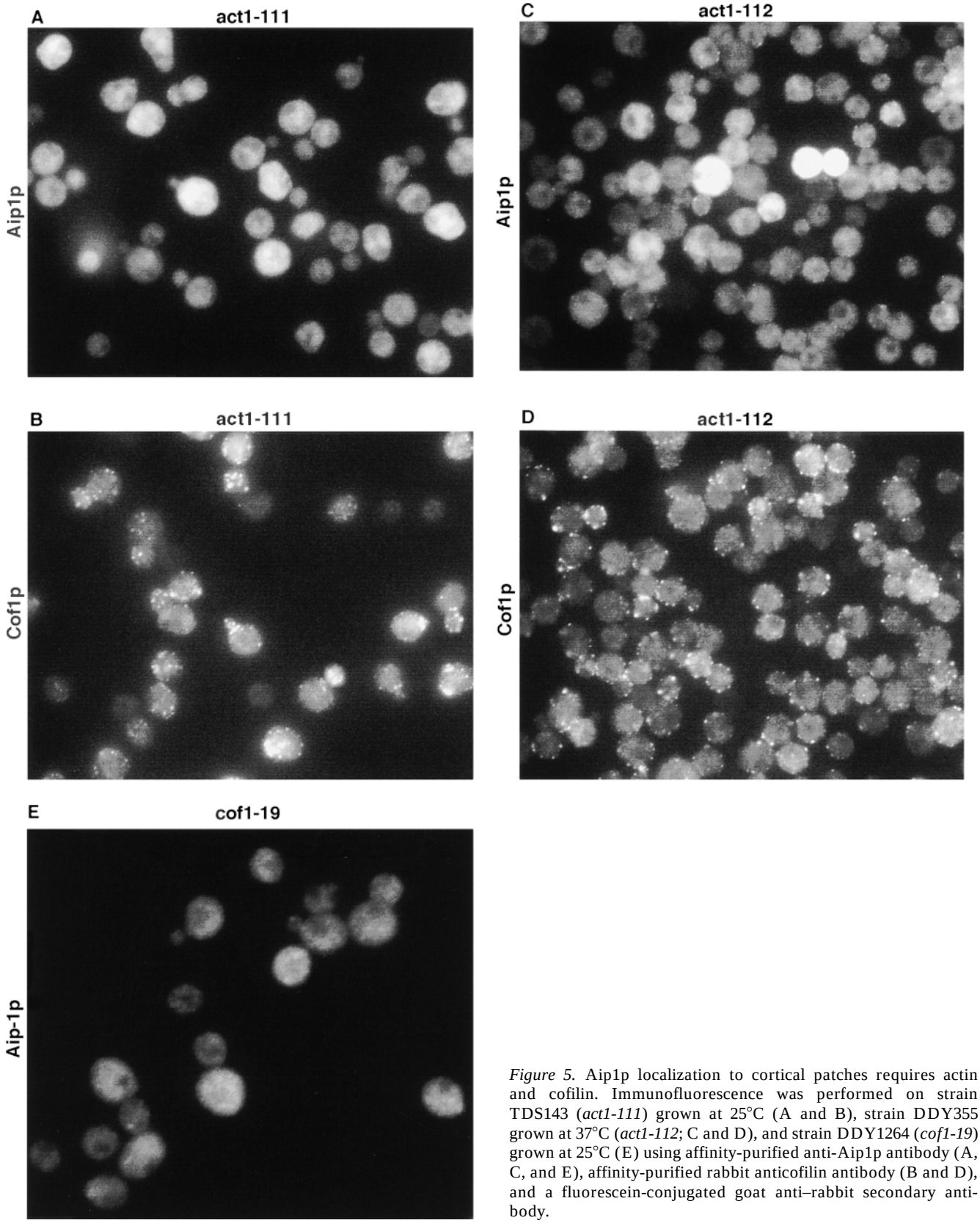

Figure 5. Aip1p localization to cortical patches requires actin and cofilin. Immunofluorescence was performed on strain TDS143 (*act1-111*) grown at 25°C (A and B), strain DDY355 grown at 37°C (*act1-112*; C and D), and strain DDY1264 (*cof1-19*) grown at 25°C (E) using affinity-purified anti-Aip1p antibody (A, C, and E), affinity-purified rabbit anticofilin antibody (B and D), and a fluorescein-conjugated goat anti–rabbit secondary antibody.

effects of stoichiometry on the Aip1p-dependent shift by varying the concentration of Aip1p (0.012–2.5 μM; Fig. 7 A, lanes 2–6) or cofilin (0.12–2.5 μM; Fig. 7 B, lanes 3–7) in cosedimentation assays with constant concentrations of F-actin (2.5 μM). Intriguingly, though the shift into the supernatant showed a linear dependence on cofilin, it did not require Aip1p at similar stoichiometry. In fact, a significant shift occurred at molar ratios of Aip1p/cofilin/actin as low as 1:50:50 (Fig. 7 A, lane 4), and can even be seen at molar ratios of Aip1p/cofilin/actin as low as 1:200:200 (Fig. 7 A, lane 6).

F-Actin Binding of Aip1p Is Facilitated by Cofilin

We used radiolabeled in vitro–translated Aip1p to evaluate binding to F-actin at a low concentration of Aip1p, which would not promote net disassembly of the filaments. The in vitro–translated Aip1p product sedimented with actin filaments. This cosedimentation was abolished by addition of excess nonradiolabeled Aip1p or by dilution of the sample, suggesting that the binding is specific (data not shown). To establish the dependence of this binding on cofilin, we pelleted increasing concentrations of actin filaments with or without stoichiometric cofilin with in vitro–translated Aip1p. Aip1p cosedimented with the F-actin in the absence of added cofilin, but addition of 1:1 cofilin increased the amount that cosedimented (Fig. 8 A). The binding of Aip1p to cofilin–F-actin is saturatable with a K_d of ~4 μM. Similar results were obtained by Western blot analysis of identical experiments with purified Aip1p (data

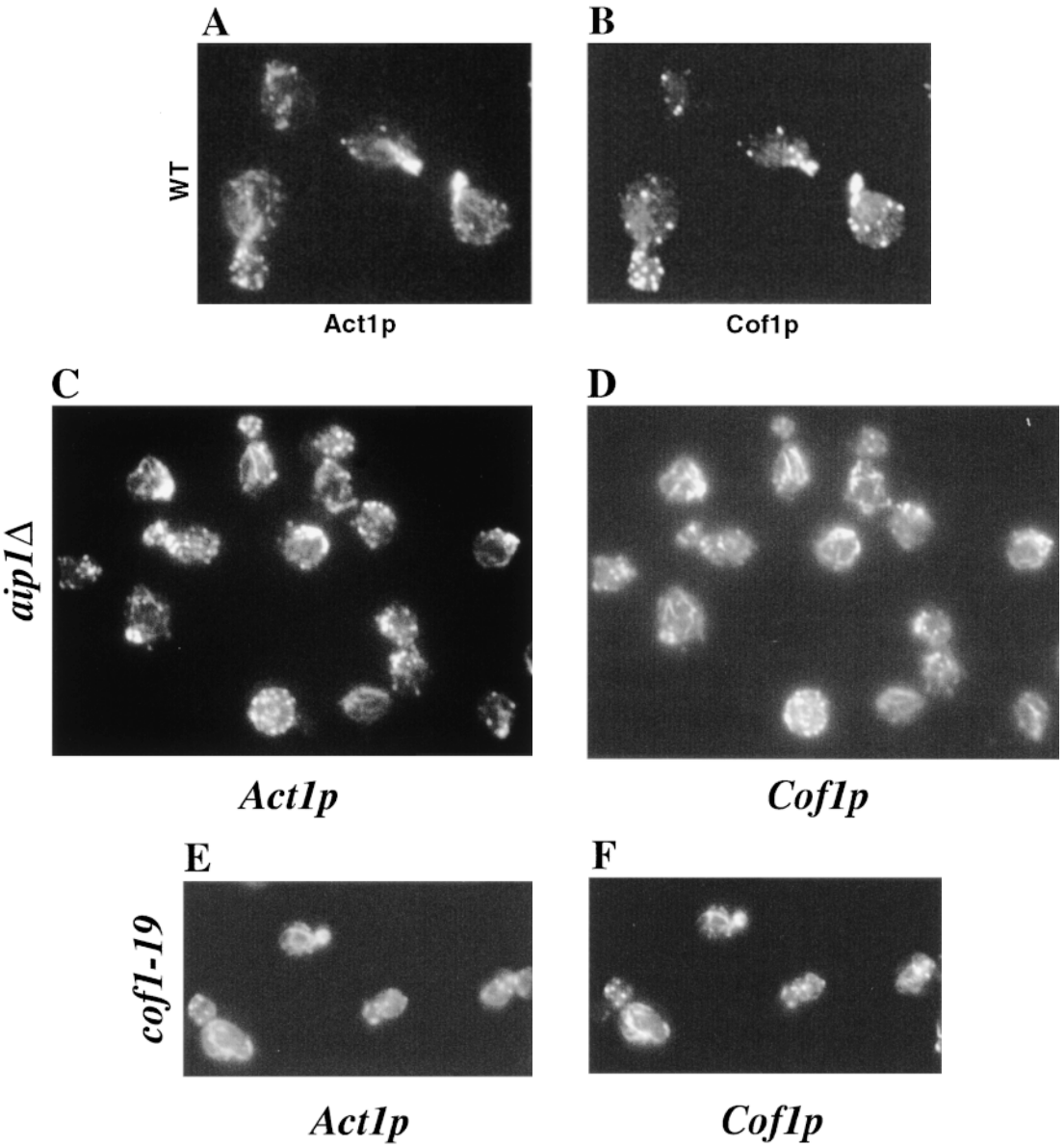

Figure 6. Selective localization of cofilin to cortical patches is dependent on Aip1p. Immunofluorescence was performed on wild-type strain DDY1252 (A and B), *aip1Δ* strain DAY30 (C and D), and on *cof1-19* strain DDY1264 (E and F) using guinea pig antiactin antibodies and a rhodamine-conjugated goat anti–guinea pig secondary antibody (A, C, and E), and anticofilin antibodies in conjunction with an FITC-conjugated goat anti–rabbit secondary antibody (B, D, and F).

not shown). We next examined how much added cofilin was required to get the increased binding. The amount of Aip1p cosedimenting with 7.5 μM F-actin falls off linearly with cofilin concentration (Fig. 8 B). Aip1p cosedimentation with F-actin could be increased in the presence of cofilin either because cofilin creates more binding sites for Aip1p, or because cofilin increases the affinity of Aip1p for actin. To distinguish between these possibilities, we added 15 and 45 nM purified Aip1p to 5 μM cofilin-saturated actin filaments (which is below the concentration that saturates Aip1p binding) and ran the sedimentation reaction. A threefold higher concentration of Aip1p increases the fraction of Aip1p cosedimenting with actin, suggesting that Aip1p binding sites are not saturated, and that the cofilin-dependent increase in binding reflects an increased affinity of Aip1p for F-actin in the presence of cofilin (data not shown). To determine stoichiometries of these proteins in yeast cells, we estimated the ratio of Aip1p/cofilin/actin in the cell by comparing immunoblots of whole-cell extracts and purified proteins of known concentration (data not shown). Aip1p, cofilin, and actin are each present in whole-cell extracts at a ratio of about 1:1:5 or 1:1:10.

Discussion

Aip1p–Cofilin–Actin Interactions Suggest a Ternary Complex

Aip1p was originally identified by its two-hybrid interaction with actin (Amberg et al., 1995a). Further two-hybrid analysis revealed an interaction between Aip1p and cofilin (Fig. 2) raising the possibility that actin, Aip1p, and cofilin might form a ternary complex. The existence of such a ternary complex is supported by evidence that Aip1p and cofilin are dependent on each other and on actin for their correct localization in vivo (Fig. 5). Binding experiments with purified proteins also support an Aip1p–cofilin–actin complex (Fig. 8). Binding of purified or in vitro–translated Aip1p to F-actin is concentration-dependent and increases at high ratios of cofilin/actin. Since cofilin is a contaminant in yeast actin preparations, despite efforts to deplete it (~1 μM/100 μM actin), we cannot rule out the possibility that contaminating native cofilin is responsible for the baseline binding to F-actin in the absence of added recombinant cofilin. Thus, it is possible that Aip1p binding to F-actin is strictly cofilin-dependent. We were unable to show a direct interaction between Aip1p and cofilin and/or G-actin by native gel shift or by cosedimentation with GST–Aip1p, further suggesting that Aip1p interacts with cofilin on F-actin.

A large set of mutations in both actin (Wertman et al., 1992) and cofilin (Lappalainen et al., 1997) was used in conjunction with the two-hybrid system to identify regions of actin and cofilin involved in the Aip1p interaction (Fig. 3). Those data that describe the cofilin–actin interface appear sound since they agree with similar studies using biochemical (Lappalainen et al., 1997), modeling (Wriggers et al., 1998), and structural (Amy McGough, personal communication) approaches. The binding footprint (as obtained by two-hybrid analysis) for Aip1p on the surface of actin (Fig. 3 B, blue and red) partially overlaps with the

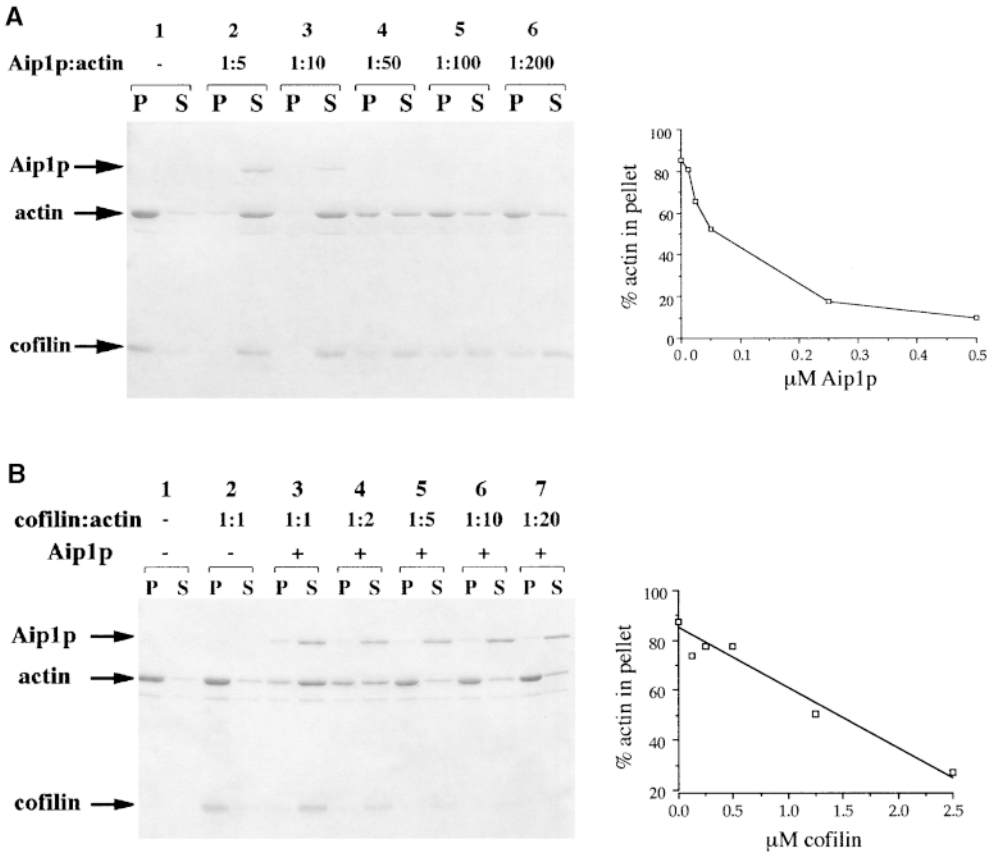

Figure 7. Aip1p enhances the extent and rate of cofilin-mediated actin dynamics. 2.5 μM actin filaments were incubated with varying concentrations of cofilin and/or Aip1p. Coomassie stained gels and accompanying quantification show the dependence of the Aip1p–cofilin interaction on Aip1p concentration (A) and on cofilin concentration (B).

cofilin binding site (red). Similarly, the footprints of Aip1p and actin on cofilin overlap as four cofilin mutants were specifically defective for both Aip1p and actin binding. Though overlapping interaction interfaces are consistent with both competitive interactions and a ternary complex, we favor the latter model because it is consistent with the localization and in vitro binding data discussed above.

While most of our structural data can be incorporated into a coherent model for interaction in a ternary complex, there were several discrepancies between the biochemical and two-hybrid data. First, only by two-hybrid assay was *cof1-9* defective for binding to actin. Additionally, although *cof1-6* has a wild-type growth phenotype, by two-hybrid analysis it appears to be completely defective for actin binding. This interaction has not been tested biochemically. These discrepancies may be an artifact resulting from the fusion to Gal4p in the two-hybrid system. Alternatively, the cofilin-actin two-hybrid interaction might be subtly different than that observed in vitro with purified components. Note that *cof1-19* is the only cofilin mutant that is defective for Aip1p localization, but it appears to interact well with both Aip1p and actin by two-hybrid analysis. This cofilin mutant may interact well with actin and Aip1p in the two-hybrid complex but have subtly altered binding properties in vivo.

In Vivo Interactions Support a Role for Aip1p in Promoting Actin Dynamics

Though the *AIP1* deletion mutant has no obvious phenotype on its own, allele-specific synthetic lethality was observed between *aip1Δ* and *act1-159*, *cof1-4*, *cof1-5*, *cof1-22*, and *cof1-6* (at 37°C). These results suggest that in the double mutants, a common function is compromised enough that cell viability is lost. Because *act1-159*, *cof1-5*, and *cof1-22* have all been shown to decrease the rate of F-actin disassembly in vivo (Lappalainen and Drubin, 1997; Belmont and Drubin, 1998), we postulate that Aip1p also promotes actin filament turnover. This conclusion is supported by our biochemical studies of Aip1p that demonstrate that it causes cofilin-dependent actin filament disassembly (Fig. 7). Note that Cof1-22p has defects in actin binding in vitro, but that Cof1-5p does not (Lappalainen et al., 1997), suggesting that the synthetic interaction is not simply a function of compromised actin binding by cofilin. The cofilin–actin interaction has not been tested biochemically for *cof1-4* or for *cof1-6*.

Specific sorting of cofilin to cortical patches but not cytoplasmic cables is lost in *aip1Δ* (Fig. 6 C) and *cof1-19* (Fig. 6 E) strains. One model that could explain these results in terms of the in vitro effects of Aip1p on actin filaments assumes that two populations of actin cables, one cofilin-bound and one tropomyosin-bound, form in yeast cells. Cofilin-bound cables would undergo net depolymerization in the presence of Aip1p, as occurs for purified actin filaments in vitro. Tropomyosin, which is localized to actin cables (Liu and Bretscher, 1989), can compete for cofilin binding sites on actin (Bernstein and Bamburg, 1982). Thus, tropomyosin would stabilize a subset of cables against Aip1p–cofilin depolymerization and these would go on to be the normal cables visualized in cells. In the *aip1Δ* strain or in a cofilin mutant that mislocalizes Aip1p (*cof1-19*), Aip1p would not be able to function synergistically with cofilin to destabilize the filaments, and both cofilin-bound and tropomyosin-bound populations of filaments would be maintained. In support of this model, cofilin also localizes to rare actin cables in *act1-159 tpm1*Δ and *act1-159 mdm20*Δ double mutant strains (Belmont et al., 1998), which would be predicted to have hyperstable F-actin structures that would not be readily disassembled by cofilin–Aip1p.

The *aip1Δ* allele was also found to enhance the defects observed in specific actin mutants (*act1-119*, *act1-125*, and *act1-133*) and in null alleles of genes encoding several components of the cortical actin cytoskeleton (Sac6p, Sla1p, and Cap2p). We believe that these double mutants most likely suffer from a general, cumulative derangement of the actin cytoskeleton, a conclusion that further supports that the actin cytoskeleton is affected in the *aip1Δ* strain.

The Aip1p–Cofilin–Actin Complex Promotes Disassembly In Vitro

We demonstrated that Aip1p causes cofilin-mediated ac-

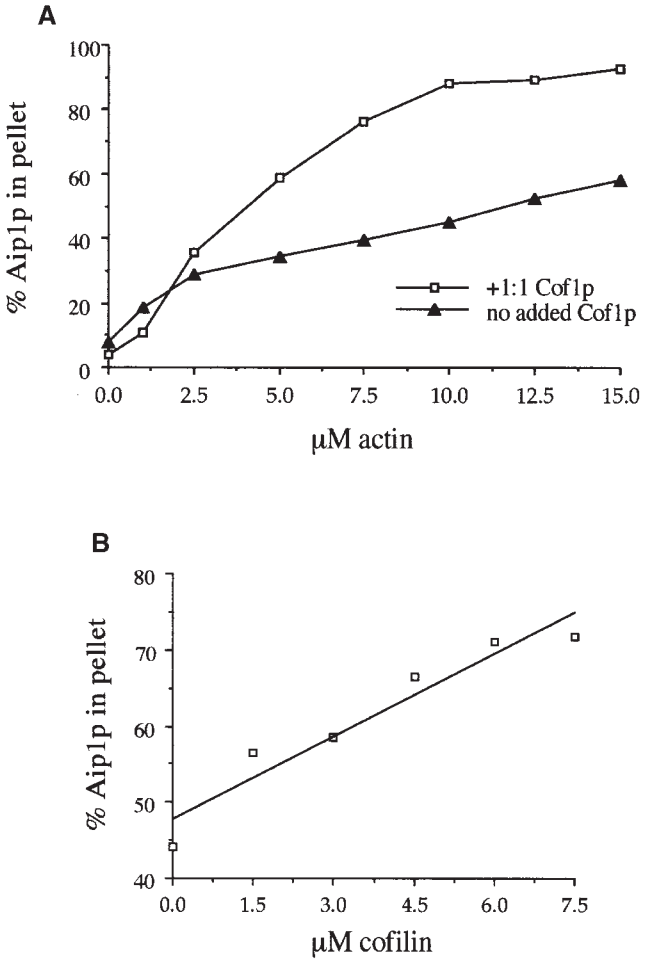

Figure 8. Aip1p actin binding is enhanced by cofilin. Actin filaments were assembled and incubated with cofilin and in vitro–translated Aip1p. A shows binding curves with and without added cofilin. B shows cosedimentation of Aip1p with 7.5 μM actin at various concentrations of cofilin.

tin filament depolymerization in vitro (Fig. 7). Interestingly, we discovered that Aip1p can induce cofilin-mediated actin filament depolymerization at stoichiometries as low as 1:50:50 Aip1/actin/cofilin. On the other hand, cofilin must be present at a 1:1 ratio with actin for optimal Aip1p-mediated activation of depolymerization.

Though we were able to detect concentration-dependent F-actin cosedimentation of Aip1p at a low molar ratio with actin (by Western blot analysis or using in vitro–translated Aip1p), we were unable to detect cosedimentation at higher Aip1p/actin ratios. One hypothesis that explains these results is that Aip1p saturates binding at a low stoichiometry with F-actin. A second hypothesis is that high ratios of cofilin/actin are required for Aip1p binding, but that at high concentrations of Aip1p, net depolymerization prevents cosedimentation of Aip1p with actin. A model that is consistent with substoichiometric or cofilin-dependent filament binding, net filament depolymerization, and the two-hybrid footprinting data is that Aip1p enhances the weak severing activity of cofilin (MacIver et al. 1991; McGough et al., 1997).

Aip1p is the first protein aside from actin and LIM-kinase to show a physical interaction with cofilin. The fact that Aip1p is highly conserved in eukaryotes suggests that it may be a cofactor for cofilin activity in all eukaryotic cells. Though the mechanistic details of these interactions remain to be elucidated fully, our biochemical data demonstrate clearly that Aip1p stimulates cofilin-mediated actin filament disassembly and our genetic and cell biological data provides powerful evidence for the relevance of this activity in vivo.

We thank Steve Elledge, Fred Winston, and David Botstein for providing strains. Phil Hieter provided the yeast genomic library used to clone *AIP1* and Tom Duncan assisted with modeling the actin and cofilin footprints. We thank Bruce Goode, Lisa Belmont, and Iain Cheeseman for their helpful criticisms and intellectual input.

Research in D.C. Amberg's laboratory was supported by National Institutes of Health (NIH) grant GM56189. Research in D.G. Drubin's laboratory was supported by NIH grant GM42759 and A.A. Rodal was supported by a Howard Hughes Medical Institute Predoctoral Fellowship.

Received for publication 12 November 1998 and in revised form 5 May 1999.

References

Adams, A.E., and J.R. Pringle. 1984. Relationship of actin and tubulin distribution to bud growth in wild-type and morphogenic-mutant *Saccharomyces cerevisiae*. *J. Cell Biol.* 98:934–945.

Adams, A.E., J.A. Cooper, and D.G. Drubin. 1993. Unexpected combinations of null mutations in genes encoding the actin cytoskeleton are lethal in yeast. *Mol. Biol. Cell.* 4:459–468.

Amberg, D.C. 1998. Three-dimensional imaging of the yeast actin-cytoskeleton through the budding cell-cycle. *Mol. Biol. Cell.* 9:3259–3262.

Amberg, D.C., E. Basart, and D. Botstein. 1995a. Defining protein interactions with yeast actin in vivo. *Nat. Struct. Biol.* 2:28-35.

Amberg, D.C., D. Botstein, and E.M. Beasley. 1995b. Precise gene disruption in *Saccharomyces cerevisiae* by double fusion PCR. *Yeast.* 11:1275–1280.

Bai, C., and S.J. Elledge. 1996. Gene identification using the yeast two-hybrid system. *Methods Enzymol.* 273:331–347.

Becker, D.M., and L. Guarante. 1991. High-efficiency transformation of yeast by electroporation. *In* Guide to Yeast Genetics and Molecular Biology. Vol. 194. C. Guthrie and G.R. Fink, editors. Academic Press, Inc., San Diego, CA. 182–186.

Belmont, L.D., and D.G. Drubin. 1998. The yeast V159N actin mutant reveals roles for actin dynamics in vivo. *J. Cell Biol.* 142:1289–1299.

Bernstein, B.W., and J.R. Bamburg. 1982. Tropomyosin binding to F-actin protects the F-actin from disassembly by brain actin-depolymerizing-factor (ADF). *Cell Motil.* 2:1–8.

Drubin, D.G., K.G. Miller, and D. Botstein. 1988. Yeast actin-binding proteins: evidence for a role in morphogenesis. *J. Cell Biol.* 107:2551–2561.

Federov, A.A., P. Lappalainen, E.V. Federov, D.G. Drubin, and S.C. Almo. 1997. Structure determination of yeast cofilin. *Nat. Struct. Biol.* 4:366–369.

Fong, H.K., J.B. Hurley, R.S. Hopkins, R. Miake-Lye, M.S. Johnson, R.F. Doolittle, and M.I. Simon. 1986. Repetitive segmental structure of the transducin beta subunit: homology with the CDC4 gene and identification of related mRNAs. *Proc. Natl. Acad. Sci. USA.* 83:2162–2166.

Goode, B.L., D.G. Drubin, and P. Lappalainen. 1998. Regulation of the cortical actin cytoskeleton in budding yeast by twinfilin, a ubiquitous actin monomer-sequestering protein. *J. Cell Biol.* 142:723–733.

Goode, B.L., J.J. Wong, A.-C. Butty, M. Peter, A.L. McCormack, J.R. Yates, D.G. Drubin, and G. Barnes. 1999. Coronin promotes rapid assembly and cross-linking of actin filaments and may link the actin and microtubule cytoskeletons in yeast. *J. Cell Biol.* 144:83–98.

Harlow, E., and D. Lane. 1988. Antibodies: A Laboratory Manual. Cold Spring Harbor Laboratory Press, Cold Spring Harbor, New York. 726 pp.

Holtzman, D.A., S. Yang, and D.G. Drubin. 1993. Synthetic-lethal interactions identify two novel genes, SLA1 and SLA2, that control membrane cytoskeleton assembly in *Saccharomyces cerevisiae*. *J. Cell Biol.* 122:635–644.

Holtzman, D.A., K.F. Wertman, and D.G. Drubin. 1994. Mapping actin surfaces required for functional interactions in vivo. *J. Cell Biol.* 126:423–432.

Lappalainen, P., and D.G. Drubin. 1997. Cofilin promotes rapid actin filament turnover in vivo. *Nature.* 388:78–82.

Lappalainen, P., E.V. Federov, A.A. Federov, S.C. Almo, and D.G. Drubin. 1997. Essential functions and actin-binding surfaces of yeast cofilin revealed by systematic mutagenesis. *EMBO (Eur. Mol. Biol. Organ.) J.* 16:5520–5530.

Liu, H., and A. Bretscher. 1989. Disruption of the single tropomyosin gene in yeast results in the disappearance of actin cables from the cytoskeleton. *Cell.* 57:233–242.

MacIver, S.K., H.G. Zot, and T.D. Pollard. 1991. Characterization of actin filament severing by actophorin from *Acanthamoeba castellani*. *J. Cell Biol.* 115: 1611–1620.

Matsumoto, S., M. Ogawa, T. Kasakura, Y. Shimada, M. Mitsui, M. Maruya, M. Isohata, I. Yahara, and K. Murakami-Murofushi. 1998. A novel 66-kDa stress protein p66, associated with the process of cyst formation of *Physarum polycephalum* is a *Physarum* homologue of a yeast actin-interacting protein AIP1. *J. Biochem.* 124:326–331.

McGough, A., B. Pope, W. Chiu, and A. Weeds. 1997. Cofilin changes the twist of F-actin: implications for actin filament dynamics and cellular function. *J. Cell Biol.* 138:771–781.

Mitchell, D.A., T.K. Marshall, and R.J. Deschenes. 1993. Vectors for the inducible overexpression of glutathione S-transferase fusion proteins in yeast. *Yeast.* 9:715–723.

Moon, A.L., P.A. Janmey, K.A. Louie, and D.G. Drubin. 1993. Cofilin is an essential component of the yeast cortical cytoskeleton. *J. Cell Biol.* 120:421–435.

Moon, A., and D.G. Drubin. 1995. The ADF/cofilin proteins: stimulus-responsive modulators of actin dynamics. *Mol. Biol. Cell.* 6:1423–1431.

Mulholland, J., D. Preuss, A. Moon, A. Wong, D. Drubin, and D. Botstein. 1994. Ultrastructure of the yeast actin cytoskeleton and its association with the plasma membrane. *J. Cell Biol.* 125:381–391.

Peranen, J., M. Rikkonen, M. Hyvonen, and L. Kääriäinenen. 1996. T7 vectors with a modified T7lac promoter for expression of proteins in *Escherichia coli*. *Anal. Biochem.* 236:371–373.

Pringle, J.R., A.E.M. Adams, D.G. Drubin, and B.K. Haarer. 1991. Immunofluorescence methods for yeast. *In* Guide to Yeast Genetics and Molecular Biology. Vol. 194. C. Guthrie and G.R. Fink, editors. Academic Press, Inc., San Diego. 565–601.

Rose, M.D., F.M. Winston, and P. Hieter. 1989. Methods in Yeast Genetics: A Laboratory Course Manual. Cold Spring Harbor Laboratory Press, Cold Spring Harbor, NY. 198 pp.

Smith, D.B., and K.S. Johnson. 1988. Single-step purification of polypeptides expressed in *Escherichia coli* as fusions with glutathione S-transferase. *Gene.* 67:31–40.

Wertman, K.F., D.G. Drubin, and D. Botstein. 1992. Systematic mutational analysis of the yeast *ACT1* gene. *Genetics.* 132:337–350.

Winston, F., C. Dollard, and L.L. Rioupero-Hovasse. 1995. Construction of a set of convenient *Saccharomyces cerevisiae* strains that are isogenic to S288C. *Yeast.* 11:53–55.

Wriggers, W., J.X. Tang, T. Azuma, P.W. Marks, and P.A. Janmey. 1998. Cofilin and gelsolin segment-1: molecular dynamics simulation and biochemical analysis predict a similar actin binding mode. *J. Mol. Biol.* 282:921–932.